

## Article

# Casimir Effect between Superconducting Plates in the Mixed State

Norio Inui 

Graduate School of Engineering, University of Hyogo, Shosha 2167, Himeji 671-2201, Hyogo, Japan;  
inui@eng.u-hyogo.ac.jp

**Abstract:** The Casimir effect between type-II superconducting plates in the coexisting phase of a superconducting phase and a normal phase is investigated. The dependence of the optical conductivity of the superconducting plates on the external magnetic field is described in terms of the penetration depth of the incident electromagnetic field, and the permittivity along the imaginary axis is represented by a linear combination of the permittivities for the plasma model and Drude models. The characteristic frequency in each model is determined using the force parameters for the motion of the magnetic field vortices. The Casimir force between parallel YBCO plates in the mixed state is calculated, and the dependence on the applied magnetic field and temperature is considered.

**Keywords:** Casimir effect; superconducting; quantum fluctuations; quantum magnetic flux



**Citation:** Inui, N. Casimir Effect between Superconducting Plates in the Mixed State. *Quantum Rep.* **2021**, *3*, 731–745. <https://doi.org/10.3390/quantum3040046>

Academic Editor: Rami Ahmad El-Nabulsi

Received: 31 October 2021

Accepted: 25 November 2021

Published: 29 November 2021

**Publisher's Note:** MDPI stays neutral with regard to jurisdictional claims in published maps and institutional affiliations.



**Copyright:** © 2021 by the author. Licensee MDPI, Basel, Switzerland. This article is an open access article distributed under the terms and conditions of the Creative Commons Attribution (CC BY) license (<https://creativecommons.org/licenses/by/4.0/>).

## 1. Introduction

The Casimir effect [1], which means that perfectly conductive plates attract each other due to the quantum fluctuations of the electromagnetic field in a vacuum, is an interesting macroscopic quantum effect. Based on Casimir's prediction, Lifshitz presented the generalized theory of the Casimir effect, which can be applied to dielectric bodies, including metals, and Lamoreaux [2] verified the Lifshitz theory via precise measurement of the Casimir force between metallic plates.

The Casimir force depends significantly on the optical properties of objects [3,4]. The Casimir force between various materials, such as perfectly conductive plates [5], metals [2,6], ferromagnetic materials [7,8], and metamaterials [9] has been investigated. In addition, superconductors are important materials for understanding the Casimir effect more effectively because they exhibit marked changes in conductivity and cause variations in the Casimir energy.

The detection of variations in the Casimir energy based on the change in the optical properties of superconductors was theoretically investigated by Bimonte et al. [10–12]. In these investigations, both transitions caused by changes in the temperature and external magnetic field were considered. Recent developments in the measurements of the Casimir force verified that the Casimir force exists and obeys Lifshitz's theory [2,6,13,14]. However, the measurement of the change in the Casimir energy is difficult, and experiments involving the phase transition of the superconductor are expected [14,15].

An experimental platform for measuring changes in the Casimir force between superconductive plates using a nanophotonic detection system on a chip was proposed [16,17]. Although the effect of phase transition on the Casimir force was not observed because of difficulties in aligning two superconductors, the measurement of the Casimir force between superconductive Al films was demonstrated for the first time, thereby enabling many problems to be solved concerning the Casimir effect between superconductors. For instance, it was discovered that the Casimir force measured experimentally was much smaller than the theoretical prediction value for the change in the force arisen by gravitational Casimir effect [18].

The conductivity of type-I superconductors changes abruptly as the external magnetic field increases. Initially, the magnetic field is expelled by the Meissner effect. However, the strong magnetic field above a critical magnetic field  $B_c$ , which depends on the material and temperature, diminishes the superconductivity. In the case of type-I superconductors, the superconductive region disappears completely above  $B_c$ . By contrast, in type-II superconductors, the penetrating external magnetic field increases gradually [19,20]. The center of the magnetic flux is in the normal phase, and the superconductive phase disappears gradually as the magnetic field increases. The coexisting phase, known as the mixed state or magnetic vortex state, exists between the lower critical magnetic field  $B_{c1}$  and upper critical magnetic field  $B_{c2}$ . The magnetic flux in the superconductor is quantized, and the defects in the superconductor pin the magnetic flux. The response of a superconductor in the mixed state to the irradiation of electromagnetic waves is primarily determined by the motion of the vortices.

The vortices (quantum magnetic flux) [21,22] form a lattice structure, and the propagating electromagnetic wave through the superconductor affects the vortices via the Lorentz force. In addition, the vortices interact with each other. The optical properties of superconductors are often expressed in terms of the penetration depth of the magnetic field. In the Meissner state, the magnetic field decays exponentially with the London penetration depth. The penetration depth depends on the magnetic field. In addition, in the type-II superconductor, the number of vortices increases with the external magnetic field. The dependence of the Casimir force between superconductive plates on the magnetic field can be calculated if the penetration depth can be expressed as a function of the external magnetic field. Recently, Villarreal and Caballero-Benitez theoretically investigated the Casimir force between high-Tc superconductors in the Meissner state [23,24].

Type-I superconductors, such as aluminum, are suitable for verifying the Casimir energy change because the electric properties of type-I superconductors are well understood. In contrast, many type-II superconductors, such as high-Tc superconductors, are anisotropic, and the mechanism of superconductivity is not sufficiently understood. Although many unknown factors remain in high-Tc superconductors, there are unique properties that are not found in type-I superconductors. The electric properties of type-II superconductors in the mixed state strongly depend on the dynamics of the vortices. The Casimir effect is usually determined by electric interactions with the quantum fluctuation of a vacuum. However, the Casimir effect between type-II superconductors under the external magnetic field cannot be understood without considering the interactions between the magnetic flux and the quantum fluctuation of the vacuum. Thus, measuring the Casimir force between the superconductors can provide findings on the interaction between vacuum quantum fluctuation and quantum magnetic flux.

In this study, we focused on the dependence of the Casimir force between high-Tc superconductors in the mixed state on the applied magnetic field. In particular, YBCO ( $\text{YBa}_2\text{Cu}_3\text{O}_7$ ) is chosen as an example because YBCO is a typical type-II superconductor, and the reflection data in the mixed state were measured [25]. Furthermore, the dependence of the reflectance on the external magnetic field can be understood in the dissipation in terms of vortex motion.

The remainder of this paper is organized as follows. In Section 2, we briefly explain the Lifshitz theory for the Casimir force. In Section 3, we introduce the formula established by Coffey and Clem for the penetration depth of a superconductor in the mixed state [26–28]. For simplicity, we consider the contribution of oscillating vortices but disregard the flux creep. In Section 4, the permittivity along the imaginary axis, which is required in the Lifshitz formula [29], derived from the penetration depth is presented. In addition, the dependence of permittivity on the magnetic field is explained. In Section 5, the calculation of the dependence of the Casimir force on the external magnetic field is presented. In the conclusion section, we summarize the relationship between the Casimir force and the material properties of superconductors in the mixed state.

### 2. Casimir Force between Parallel Plates

We consider two parallel semi-infinite superconductive plates. The separation distance between the plates is  $a$ , and an external magnetic field  $\mathbf{B}$  is applied vertical to the surface of the plates. The Casimir force exerted on the plates per area can be obtained by calculating the derivative of the Casimir energy with respect to  $a$ . The Casimir energy can be obtained by regularizing the zero-point energy of the electromagnetic field between the plates. The electromagnetic field between the plates is characterized by the angular frequency  $\omega$ , wave vector  $\mathbf{k} = (\mathbf{k}_\perp, k_z)$ , where  $\mathbf{k}_\perp$  is defined as the wave vector parallel to the surface and polarization  $\sigma$  (transverse magnetic mode (TM) and transverse electric mode (TE)), as shown in Figure 1.

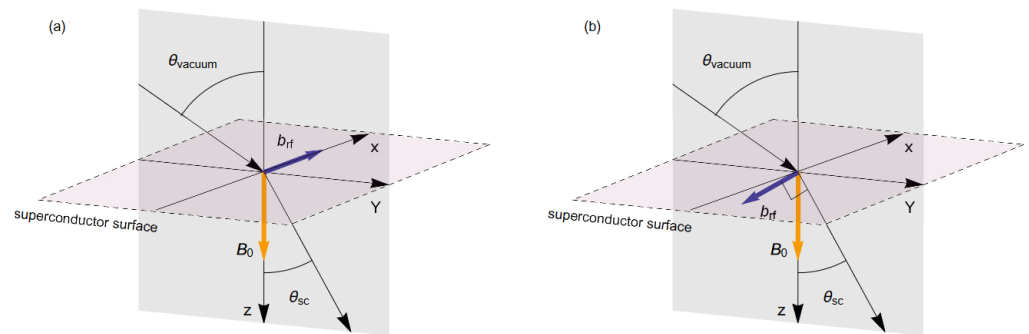


**Figure 1.** Light propagation in (a) TM mode and (b) TE mode from a vacuum to a superconductor. The  $yz$ -plane is the plane of incidence. The external magnetic field  $B_0$  is perpendicular to the surface of the superconductor. The magnetic field of the light  $\mathbf{B}_{\text{light}}$  in TM mode is perpendicular to the plane of incidence. Conversely, the electric field of the light is perpendicular to the plane of incidence, and the magnetic field exits at the  $yz$  plane.

For the TM mode, the magnetic field of the incident light  $\mathbf{B}_{\text{light}}$  is parallel to the surface of the superconductor. Thus,  $\mathbf{B}_{\text{light}}$  is orthogonal to the external magnetic field  $\mathbf{B}$  regardless of the incident angle  $\theta_{\text{vacuum}}$ . Concerning the TE mode,  $\mathbf{B}_{\text{light}}$  is parallel to the plane of incidence, and the angle between  $\mathbf{B}_{\text{light}}$  and  $\mathbf{B}$  is  $\pi/2 - \theta_{\text{vacuum}}$ .

The electromagnetic field between the plates must satisfy the following dispersion relations:

$$G_{\text{TM}}(\omega, k_\perp) \equiv \left( \frac{\epsilon(\omega)q - K}{\epsilon(\omega)q + K} \right)^{-2} e^{2aq} - 1 = 0, \tag{1}$$

$$G_{\text{TE}}(\omega, k_\perp) \equiv \left( \frac{q - K}{q + K} \right)^{-2} e^{2aq} - 1 = 0, \tag{2}$$

where  $q(\omega, k_\perp) = \sqrt{k_\perp^2 - \omega^2/c^2}$  and  $K(\omega, k_\perp) = \sqrt{k_\perp^2 - \epsilon(\omega)\omega^2/c^2}$ . The dependence of permittivity  $\epsilon(\omega)$  on the temperature and magnetic field is discussed in the next section.

By summing up the photon energy over all combinations of  $(\omega, k_\perp)$  satisfying the dispersion relations and regularizing the energy, the Casimir force per area at temperature  $T$  can be expressed by the Lifshitz formula [3,4] as follows:

$$P(a, T) = -\frac{k_B T}{\pi} \sum'_{l=0} \int_0^\infty q_l k_\perp dk_\perp \left( G_{\text{TM}}(i\xi_l, k_\perp)^{-1} + G_{\text{TE}}(i\xi_l, k_\perp)^{-1} \right), \tag{3}$$

where  $\xi_l \equiv 2\pi k_B T l / \hbar$ , ( $l = 0, 1, \dots$ ) is the Matsubara frequency and  $q_l = q(i\xi_l, k_\perp)$ . The prime on the summation symbol denotes that 1/2 should be inserted if  $l = 0$ . The material dependence on the Casimir force is determined by the permittivity along the imaginary axis. To evaluate the Casimir force, it is convenient to set the unit frequency to  $\xi_1$ , which

is the lowest positive Matsubara frequency. In addition, by defining the dimensionless wavenumber as  $y = ck_{\perp}/\xi_1$ , the Lifshitz formula can be rewritten as

$$P(\alpha, T) = -\frac{k_B T}{\pi} \left(\frac{\xi_1}{c}\right)^3 \sum_{l=0}^{\infty} \int_0^{\infty} y \sqrt{y^2 + l^2} dy \{g_{\text{TM}}^{-1}(l, y) + g_{\text{TE}}^{-1}(l, y)\}, \quad (4)$$

$$g_{\sigma}(l, y) = r_{\sigma}^2(l, y) e^{2\alpha \sqrt{y^2 + l^2}}, \quad \sigma \in \{\text{TE}, \text{TM}\}. \quad (5)$$

Here,  $\alpha \equiv a/(c/\xi_1)$  is the distance between the plates that is normalized by the unit length  $c/\xi_1$ , and the reflection coefficients are represented as

$$r_{\text{TM}}(l, y) = \frac{\epsilon_l \sqrt{y^2 + l^2} - \sqrt{y^2 + \epsilon_l l^2}}{\epsilon_l \sqrt{y^2 + l^2} + \sqrt{y^2 + \epsilon_l l^2}}, \quad (6)$$

$$r_{\text{TE}}(l, y) = \frac{\sqrt{y^2 + l^2} - \sqrt{y^2 + \epsilon_l l^2}}{\sqrt{y^2 + l^2} + \sqrt{y^2 + \epsilon_l l^2}}, \quad (7)$$

where  $\epsilon_l = \epsilon(i\xi_l)$  [4]. It is noteworthy that  $\epsilon_l l^2$  is not always zero at  $l = 0$ . If  $\lim_{\omega \rightarrow 0} \omega^2 \epsilon(\omega)$  converges to a positive value  $\omega_p^2$ , then the reflection coefficients at  $l = 0$  are  $r_{\text{TM}}(0, y) = 1$  and

$$r_{\text{TE}}(0, y) = \frac{y - \sqrt{y^2 + \omega_p^2}}{y + \sqrt{y^2 + \omega_p^2}}. \quad (8)$$

The unit frequency  $\xi_1$  at 1 K is  $8.2 \times 10^{11}$  rad/s, and its wavelength is 58  $\mu\text{m}$ . This characteristic length decreases as the temperature increases. At the phase transition temperature of YBCO (88.2 K), the wavelength decreases to 0.65  $\mu\text{m}$ .

Many high- $T_c$  superconductors are uniaxial materials, and the Casimir effect due to the anisotropy of dielectric properties is considered using the following reflection coefficients [4,30]:

$$r_{\text{TM}}(l, y) = \frac{\sqrt{\epsilon_{xl}\epsilon_{zl}} \sqrt{y^2 + l^2} - \sqrt{y^2 + \epsilon_{zl} l^2}}{\sqrt{\epsilon_{xl}\epsilon_{zl}} \sqrt{y^2 + l^2} + \sqrt{y^2 + \epsilon_{zl} l^2}}, \quad (9)$$

$$r_{\text{TE}}(l, y) = \frac{\sqrt{y^2 + l^2} - \sqrt{y^2 + \epsilon_{xl} l^2}}{\sqrt{y^2 + l^2} + \sqrt{y^2 + \epsilon_{xl} l^2}}. \quad (10)$$

where  $\epsilon_{xl}$  and  $\epsilon_{zl}$  are permittivity in the  $xy$ -plane and along the  $z$ -axis, respectively. In this study, we use these formulas to consider the anisotropy of dielectric properties caused by the magnetic flux.

### 3. Permittivity of Superconductor in the Mixed State

#### 3.1. Relationship between Conductivity and Permittivity

The optical properties required to calculate the Casimir force using the Lifshitz theory are the permittivities at arbitrary Matsubara frequencies along the imaginary axis. As shown below, the permittivity along the imaginary axis is obtained using the Hilbert transform of the imaginary part of the permittivity along the real frequency axis. Therefore, an imaginary part of the permittivity for arbitrary frequencies is necessary. However, the experimentally obtained optical data of the superconductor are limited; therefore, we introduce model functions.

The real part of conductivity  $\sigma_1(\omega)$  of superconductors below the transition temperature  $T_c$  is often expressed using the two-flow model as follows:

$$\sigma_1(\omega) = D\delta(\omega) + \sigma_{1,n}(\omega), \quad (11)$$

where  $\delta(\omega)$  is a delta function with a peak at  $\omega = 0$  and  $\sigma_{1,n}(\omega)$  is the contribution from the fluid in the normal phase. We determine the coefficient  $D$  using the sum rule of the oscillator strength. According to the sum rule [31,32], the real part is correlated to the imaginary part of conductivity  $\sigma_2$  as follows:

$$\frac{2}{\pi} \int_0^{\infty} \sigma_1(\omega) d\omega = \lim_{\omega \rightarrow \infty} \omega \sigma_2(\omega). \quad (12)$$

In the London theory framework, the imaginary part of the conductivity in the superconductive state is expressed using the London penetration depth (SI unit) as

$$\sigma_2(\omega) = \frac{1}{\mu_0 \lambda_L^2 \omega}, \quad (13)$$

where  $\mu_0$  is the permeability of vacuum. Accordingly, the coefficient  $D$  is given by

$$D = \frac{\pi}{\mu_0 \lambda_L^2}. \quad (14)$$

Using the Kramers–Kronig relation, the permittivity along the imaginary axis is expressed as

$$\epsilon(i\tilde{\zeta}) = 1 + \frac{2}{\pi \epsilon_0} \int_0^{\infty} \frac{\sigma_1(\omega)}{\omega^2 + \tilde{\zeta}^2} d\omega, \quad (15)$$

where  $\epsilon_0$  is the permittivity of the vacuum. Consequently, the contribution of the superconductive fluid to the permittivity along the imaginary frequency is expressed as

$$\epsilon(i\tilde{\zeta}) = 1 + \frac{c^2}{\lambda_L^2 \tilde{\zeta}^2}. \quad (16)$$

This implies that the permittivity in the Meissner state obeys the plasma model with plasma frequency  $\omega_{p0} = c/\lambda_L$ . According to the theory by Villarreal and Caballero-Benitez for the Casimir force between YBCO plates in the superconductive state without magnetic field, the dielectric function is expressed as follows:

$$\begin{aligned} \epsilon_s(\omega, T) = & \epsilon_{\infty} + \frac{i\pi\omega_{ps}^2(T)}{2\omega} \delta(\omega) - \frac{\omega_{ps}^2(T)}{\omega^2} \\ & - \frac{S_{ir}\omega_{ir}^2}{\omega^2 - \omega_{ir}^2 + i\gamma_{ir}\omega} - \sum_{j=1}^6 \frac{S_j\omega_j^2}{\omega^2 - \omega_j^2 + i\gamma_j\omega}. \end{aligned} \quad (17)$$

The parameters in Equation (17) are given in Ref. [23]. Although YBCO has anisotropy for the dielectric permittivity even in the absence of a magnetic field, we consider only the anisotropy arising from vortices.

### 3.2. Permittivity along the Imaginary Axis

The conductivity of metallic superconductors that obey the BCS theory can be analytically expressed in terms of the electron density, energy gap, and residual relaxation time [11]. In the case of high-Tc superconductors, it is convenient to derive the conductivity from the penetration depth. The complex conductivity can be obtained from the penetration depth  $\lambda$  using the following expression:

$$\sigma(\omega) = \frac{i}{\mu_0 \omega \lambda^2}. \quad (18)$$

The real and imaginary part of the conductivity are respectively expressed as

$$\sigma_1(\omega) = \frac{2}{\mu_0\omega} \frac{\lambda_1\lambda_2}{|\lambda|^4}, \quad (19)$$

$$\sigma_2(\omega) = \frac{1}{\mu_0\omega} \frac{\lambda_1^2 - \lambda_2^2}{|\lambda|^4}, \quad (20)$$

where  $\lambda_1$  and  $\lambda_2$  are the real and imaginary parts of the penetration depth, respectively [28].

We calculate the permittivity of the superconductor in the mixed state along the imaginary axis in a manner similar to that described in Section 3.1 for the incidence of light in the TM mode. Coffey and Clem studied the dynamics of the magnetic vortices in the mixed state induced by the radiation of electromagnetic waves [26–28] and derived the equation of motion for vortices using the viscous drag coefficient  $\eta$  and the coefficient of restoring force per unit length of the magnetic vortex  $\kappa$ . The resulting complex penetration depth of the superconductor, in which the contribution of the shaking vortices is considered, is given by

$$\lambda = \sqrt{\frac{B\phi_0}{\mu_0(\kappa - i\omega\eta)} + \lambda_L^2}, \quad (21)$$

where  $\phi_0$  is the magnetic flux quantum, which is defined as  $h/2e$  (see details in Appendix A). Using Equations (19) and (20), the components of the complex conductivity for  $\omega > 0$  are expressed as

$$\sigma_1(\omega) = \frac{1}{\mu_0\lambda_L^2} \frac{\alpha^2 - \beta^2}{\alpha(\omega^2 + \alpha^2)}, \quad (22)$$

$$\sigma_2(\omega) = \frac{1}{\mu_0\lambda_L^2\omega} \left( 1 + \frac{\beta^2 - \alpha^2}{\omega^2 + \alpha^2} \right). \quad (23)$$

Here,  $\alpha$  and  $\beta$ , which are the real and imaginary parts of  $\lambda^2$ , respectively, are defined by

$$\alpha = \frac{\kappa}{\eta} + \frac{B\phi_0}{\mu_0\eta\lambda_L^2}, \quad (24)$$

$$\beta = \sqrt{\frac{\kappa}{\eta}\alpha}. \quad (25)$$

Using  $\alpha$  and  $\beta$ , the penetration length is rewritten as

$$\lambda = \lambda_L \sqrt{\frac{\alpha^2 - \beta^2}{\beta^2 - i\alpha\omega} + 1}. \quad (26)$$

Similar to Equation (11), the conductivity for  $\omega \geq 0$  can be expressed by adding a DC term as

$$\sigma_1(\omega) = D\delta(\omega) + \frac{1}{\mu_0\lambda_L^2} \frac{\alpha^2 - \beta^2}{\alpha(\omega^2 + \alpha^2)}. \quad (27)$$

The summation of  $\sigma_1$  over the frequency is

$$\int_0^\infty \sigma_1(\omega) d\omega = \frac{D}{2} + \frac{\pi(\alpha^2 - \beta^2)}{2\mu_0\lambda_L^2\alpha^2}. \quad (28)$$

Since  $\lim_{\omega \rightarrow \infty} \omega \sigma_2(\omega) = 1/\mu_0 \lambda_L^2$ , using Equations (12) and (28), the sum rule [31,32] yields

$$D = \frac{\pi \beta^2}{\mu_0 \lambda_L^2 \alpha^2}. \quad (29)$$

The vortices do not displace along the z-axis. Thus, we determine the permittivity for the TM mode along the imaginary axis of the superconductor in the mixed state as

$$\epsilon_x(i\tilde{\zeta}) = 1 + \frac{\omega_p^2}{\tilde{\zeta}^2} + \frac{\omega_D^2}{\tilde{\zeta}(\tilde{\zeta} + \alpha)}, \quad (30)$$

$$\epsilon_z(i\tilde{\zeta}) = 1 + \frac{\omega_{p0}^2}{\tilde{\zeta}^2}. \quad (31)$$

The second and third terms of (30) represent the permittivities of the plasma and the Drude models, respectively. The plasma frequencies  $\omega_p$  and  $\omega_D$  are respectively expressed as

$$\omega_p = \frac{c}{\lambda_L} \left( \frac{\beta}{\alpha} \right), \quad (32)$$

$$\omega_D = \frac{c}{\lambda_L} \sqrt{1 - \left( \frac{\beta}{\alpha} \right)^2}. \quad (33)$$

We consider the dependence of  $\omega_p$  and  $\omega_D$  of YBCO on the temperature and magnitude as examples. The external magnetic field is applied vertically to the *ab*-plane. The dependences of  $\lambda_L$ ,  $\eta$ , and  $\kappa$  on the reduced temperature  $t = T/T_c$  and the magnetic field, provided in Ref. [28,33,34], are as follows:

$$\lambda_L(t, B) = \frac{\lambda_0}{\sqrt{1-t^4} \sqrt{1 - \frac{B}{B_{c2}(t)}}}, \quad (34)$$

$$\eta(t) = \frac{\phi_0 B_{c2}(t)}{\rho(t)}, \quad (35)$$

$$\kappa(t) = \kappa_0 \left[ 1 - \left( \frac{T_c t}{T_{c2}} \right)^2 \right]^2, \quad (36)$$

where  $\lambda_0$ ,  $\kappa_0$ , and  $T_{c2}$  are parameters determined by experiments. The parameters of the YBCO are summarized in Table 1 [28].

**Table 1.** Parameters for vortex dynamics [28].

$T_c$	88.2 K
$T_{c2}$	87 K
$\lambda_0$	140 nm
$B_{c2,0}$	112 T
$\kappa_0$	$2.1 \times 10^4$ N/m <sup>2</sup>
$c_0$	$2.0 \times 10^{-7}$ $\Omega$ m
$c_1$	$9.7 \times 10^{-7}$ $\Omega$ m/K

The functions of the upper critical magnetic field  $B_{c2}(t)$  and the resistivity in the normal state  $\rho(t)$  [34] are defined as

$$B_{c2}(t) = \frac{B_{c2,0}(1 - t^2)}{1 + t^2}, \tag{37}$$

$$\rho(t) = c_1 t + c_0. \tag{38}$$

The magnetic dependence of the penetration depth arises from that of  $f_0$  and  $\lambda_L$ . Although the obtained Formulas (30) and (31) for permittivity are valid for  $B_{c1} < B < B_{c2}$ , where the lower critical magnetic field  $B_{c1}$  is approximately 0.25 T for YBCO [33], we have the values in the absent of the magnetic field,  $\omega_p = c/\lambda_L$  and  $\omega_D = 0$ , by setting it to be  $B = 0$ . Figure 2 shows the permittivity of the superconductor in the mixed state along the imaginary axis at  $t = 0.1$  for  $B = 0$  and 10 T. We find that the permittivity decreases below approximately  $10^{12}$  rad/s when a strong external magnetic field is applied.

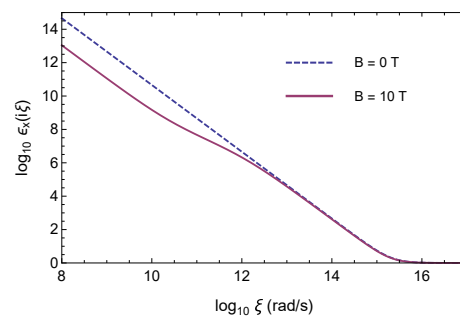


**Figure 2.** Permittivity parallel to the surface of YBCO in the mixed state at  $T = 8.82$  K ( $t = 0.1$ ) along imaginary axis in a log–log scale.

The plasma frequencies and  $\alpha$  depend on the external magnetic field. Figure 3a,b show the dependence of plasma frequencies  $\omega_p$  and  $\omega_D$  at  $t = 0.1$  and 0.5, respectively.

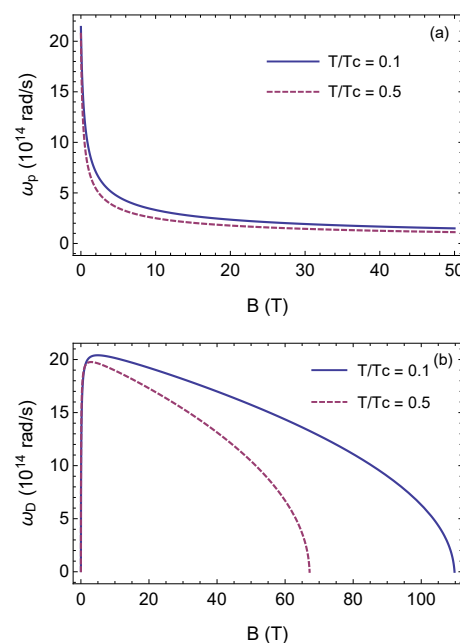


**Figure 3.** Dependence of frequencies (a)  $\omega_p$  (plasma model) and (b)  $\omega_D$  (Drude model) on magnetic field at  $t = 0.1$  (solid line) and 0.5 (dashed line).

The plasma frequency  $\omega_p$  decreases rapidly as the external magnetic field increases. By contrast,  $\omega_D$  increases rapidly and then decreases gradually as the external magnetic

field increases. Figure 4 shows that  $\omega_D$  decreases as the temperature increases. Thus, the reflection coefficients also decrease near the phase transition temperature. To obtain accurate reflection coefficients near the critical point, the flux creep, which is disregarded in this study, must be considered. In addition, the contribution of the permittivity described by the Lorentz model (as expressed in Equation (17)), which will be discussed later, must be taken into account.

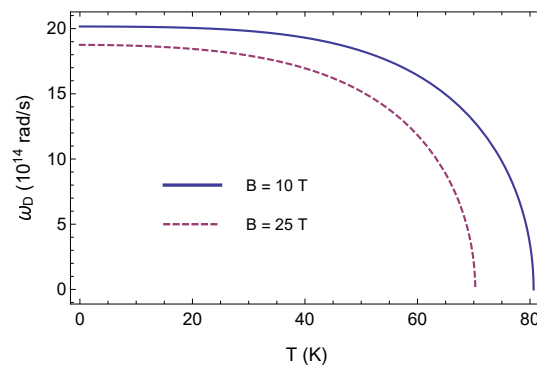


**Figure 4.** Temperature dependence of frequency  $\omega_D$  (Drude model).

In the case of the TE mode, the magnetic field propagating in a superconductor is not orthogonal to the external magnetic field, except for the angle of incidence  $\theta_{\text{vacuum}} = 0$ . According to the generalized theory by Coffey and Clem for the propagation of an electromagnetic wave in a superconductor with an oblique applied static magnetic field [35],  $\alpha$  defined in Equation (24) for the TE mode is replaced with

$$\alpha = \frac{\kappa}{\eta} + \frac{B\phi_0 \cos^2 \theta_{\text{sc}}}{\mu_0 \eta \lambda_L^2}. \quad (39)$$

Accordingly, the permittivity depends on the refracting angle  $\theta_{\text{sc}}$ . However, the contribution of the TE mode is smaller than that of the TM mode for small separation distances. For example, the ratio of the TE mode's contribution to the TM mode at  $T = 50$  K and  $B = 25$  T is approximately 0.37 at  $1 \mu\text{m}$  in the calculation presented in the next section. The ratio is reduced to 0.02 at  $0.1 \mu\text{m}$ . In addition, the contribution of large  $\theta_{\text{sc}}$  is small. To explain this, it should be emphasized that the angle  $\theta_{\text{sc}}$  is not the angle of incidence. According to Snell's law, the relationship between the refracting angle and the angle of incidence  $\theta_{\text{in}}$  of the incident light that propagates from a vacuum to a material with permittivity  $\epsilon(\omega)$  is expressed as  $\sin^{-1} \theta_{\text{in}} / \sqrt{\epsilon(\omega)}$ . Thus, if the permittivity is large, the refracting angle is small. The approximation that sets  $\theta_{\text{sc}}$  as 0, which is the basis of the surface impedance approach, is often used in the calculation of the Casimir force between metals [36]. At large frequencies, i.e., large  $l$ , the refracting angle becomes large. However, the contribution of large frequencies in the summation in Equation (4) is usually small. For these reasons, we use the approximation  $\theta_{\text{sc}} = 0$  in the following calculations.

#### 4. Effect of External Magnetic Field on Casimir Force between Superconductive Plates

We consider the Casimir force between the YBCO plates in the mixed state. The contribution of the superconductive phase of permittivity is described using the plasma model. As the external magnetic field increases, the volume in the superconductive phase decreases, resulting in a decrease in plasma frequency  $\omega_p$ . By contrast, the number of magnetic flux increases, and the contribution, which is expressed by the Drude model to the permittivity, increases. Hence, the reflection coefficient is altered by increasing the external magnetic field, thereby causing a change in the Casimir force.

To show the dependence of the Casimir force on the magnetic field, it is useful to introduce the Casimir force normalized by that between perfectly conducting plates,  $P_c(a)$ , which is expressed as:

$$P_c(a) = -\frac{\pi^2 \hbar c}{240a^4}. \quad (40)$$

Figure 5a shows the normalized Casimir force  $\eta_c \equiv P(a, T)/P_c(a)$  at a fixed separation distance  $a = 1 \mu\text{m}$  for a magnetic field between 1 and 60 T.

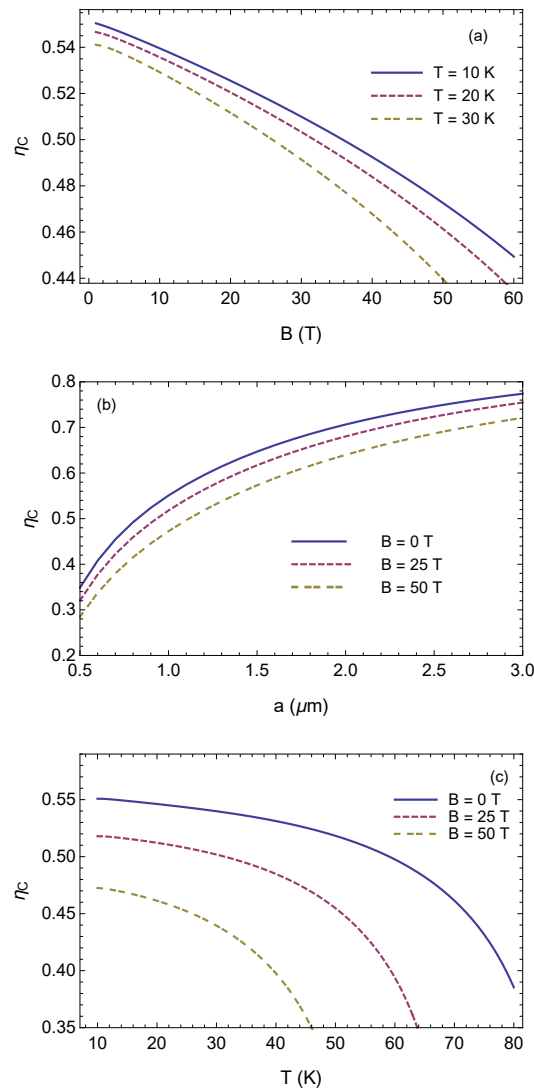


**Figure 5.** (Color online) Dependence of normalized Casimir force between YBCO plates in the mixed state on (a) magnetic field, (b) separation distance, and (c) temperature.

At higher temperatures, the normalized Casimir force decreases rapidly as the magnetic field increases. Near absolute zero, the normalized Casimir force between metallic plates, whose permittivity is described mainly by the plasma model with plasma frequency  $\omega_p$ , can be approximated as

$$\eta_c \approx 1 - \frac{16c}{3\omega_p a}, \quad (41)$$

for large separations.

Although an increase in plasma frequency  $\omega_D$  strengthens the Casimir force, the decrease in plasma frequency  $\omega_p$  is more significant in the magnetic field range of the calculation. Accordingly, the normalized Casimir force decreases monotonically owing to the external magnetic field. Combining Equations (1), (2), (9), (10), (30) and (31), we calculated the Casimir force. Figure 5b shows the dependence of  $\eta_c$  on the separation distance  $a$ . As expected (based on Equation (41)), the normalized Casimir force decreases as the external magnetic field increases for any separation distance. Figure 5c shows the temperature dependence of the normalized Casimir force. If the permittivity is independent of temperature, then the Casimir force usually increases as the temperature increases owing to the additional contributions of thermal radiation. However, the normalized Casimir force decreases, as shown in Figure 5c. Plasma frequency  $\omega_D$  decreases as the temperature increases, as shown in Figure 4, and this change affects the Casimir force more significantly than the thermal radiation.

Plasma frequency  $\omega_D$  decreases rapidly as the temperature approaches the phase transition temperature. Thus, several contributions to the permittivity that were disregarded, such as the contribution described by the Lorentz model presented as the third term in Equation (17), must be considered. However, if the additional terms are independent of the temperature and magnetic field, then the dependence of the Casimir force on the magnetic field and temperature is qualitatively unchanged. A comparison of the temperature dependence of the Casimir force of the YBCO plate with and without the Lorentz term is shown in Figure 6. The Casimir force is increased by adding a Lorentz term. In particular, the decrease due to the increase in temperature is suppressed by the addition of the Lorentz term.

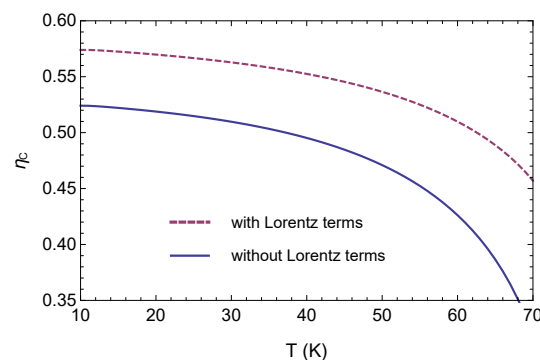


**Figure 6.** Comparison between normalized Casimir force acting on the superconductive plates with and without terms based on the Lorentz model.

## 5. Conclusions

The penetration depth of the magnetic field is one of the most important parameters for characterizing the superconducting state. We expressed the conductivity of superconductors in terms of penetration depth and obtained the permittivity along the imaginary frequency using the Kramers–Kronig relation. The permittivity was expressed as a combination of functions that are typically used in the plasma and Drude models. Each contribution changed depending on the applied magnetic field and temperature. The ratio of parameters  $\alpha$  and  $\beta$  defined in (24) and (25) governed the change in the plasma frequency. The ratio  $\beta/\alpha$  is expressed as  $(1 + f_0/\kappa\lambda_L^2)^{-1/2}$ . In particular, at  $T = 0$ , the ratio was approximately  $(1 + c_B B)^{-1/2}$  near  $B = 0$ , where  $c_B = \phi_0/\mu_0\kappa_0\lambda_0^2$ . The value of  $c_B$  for YBCO is  $4 \text{ T}^{-1}$ . It is noteworthy that the ratio is independent of the viscous drag coefficient, which affects the relaxation time.

The superconductivity term in the conductivity was expressed using a delta function, and the plasma frequency of the permittivity was determined from the coefficient of the delta function using the sum rule. As the external magnetic field increased, the conductivity of the superconductive component decreased and the plasma frequency

decreased. Meanwhile, the contribution in the normal phase, which is associated with the motion of the magnetic flux quantum increased. The motion of the magnetic fluxes was determined by solving an interacting oscillator model with viscous drag, and its amplitude was expressed in terms of the viscous drag and restoring force coefficient, which was regarded as a spring constant. Subsequently, the penetration depth was determined from the amplitude of the oscillator, and the material dependence of the plasma frequencies was determined from the spring constant.

If the spring constant is small, then the plasma frequency will be sensitive to the external magnetic field. The spring constant of a polycrystalline superconductor is reported to be  $10^3$  to  $10^4$  smaller than that of a single crystal [33]. Hence, the magnetic dependence of the Casimir force between polycrystalline superconductors might differ from that presented here. In addition, the spring constant decreases as the temperature increases. In particular, the spring constant changes significantly near the critical temperature. Accordingly, the Casimir force changes significantly near the critical temperature.

The material dependence of the relaxation parameter in the Drude model was determined based on the electrical resistivity in the normal phase. The temperature dependence of the electrical resistivity was obtained by extrapolating the experimental data below the transition temperature [34]. The extrapolated value at absolute zero is large in comparison with those of metallic superconductors and almost equal to the conductivity of lead at 20 °C; thus, the relaxation parameter also affects the change in the Casimir force.

The modulation of the Casimir force by changing the material properties has attracted attention [37]. An example is the Casimir force between a gold sphere and Si membrane by irradiating laser pulses [38]. The plasma frequency is proportional to the square root of the charge carrier concentration. Thus, the increase in electrons and holes created by irradiation results in the plasma frequency and enhances the Casimir force. As another example, the change in the optical transparency of Ni-Mg films by exposure of hydrogen was used in the modification of the Casimir force [39]. By measuring the change in the Casimir force, we may gain a deeper understanding of both the Casimir force and material properties. For superconductors, optical conductors have not been sufficiently investigated for electromagnetic waves with frequencies higher than those of microwaves. Hence, by measuring the Casimir force exerted on the superconductor (particularly for small separation distances), which depend on the conductivity at higher frequencies, the optical properties of the superconductor can be considered.

**Funding:** This research was funded by the Ministry of Education, Culture, Sports, Science and Technology, Grant-in-Aid for Scientific Research (C), MEXT KAKENHI Grant Number 21K04895.

**Institutional Review Board Statement:** Not applicable.

**Informed Consent Statement:** Not applicable.

**Data Availability Statement:** Not applicable.

**Acknowledgments:** This research was supported by the Ministry of Education, Culture, Sports, Science and Technology, Grant-in-Aid for Scientific Research(C), MEXT KAKENHI Grant Number 21K04895.

**Conflicts of Interest:** The author declares no conflict of interest.

## Appendix A. Derivation of the Penetration Depth

The penetration depth of a superconductor in the mixed state for light whose magnetic field is orthogonal to the external magnetic field, is derived on the basis of the theory developed by Coffey and Clem [35]. Without loss of generality, we can assume that the propagating magnetic field is parallel to the  $x$ -axis, as shown in Figure 1a. We express the current parallel to the  $y$ -axis,  $J_y$ , in two ways. First, the magnetic field exponentially decays owing to the Meissner effect, and the amplitude at time  $\tau$  is expressed using a complex penetration depth  $\lambda_z$  as

$$\mathbf{h}(z, \tau) = h_0 e^{-\frac{z}{\lambda_z}} e^{-i\omega\tau} \mathbf{e}_x, \quad (\text{A1})$$

where  $\mathbf{e}_\zeta$  ( $\zeta \in \{x, y, z\}$ ) is the unit vector along the  $\zeta$ -axis. Using Ampere's law, the current along the  $y$ -axis is induced, and its density is given by

$$\mathbf{J}_y(z, \tau) = -\frac{h_0}{\lambda_z} e^{-\frac{z}{\lambda_z}} e^{-i\omega\tau} \mathbf{e}_y. \quad (\text{A2})$$

The vortex experiences the Lorentz force:

$$\mathbf{F}(z, \tau) = \mathbf{J}_y(z, \tau) \times \phi_0 \mathbf{e}_z. \quad (\text{A3})$$

The direction of the Lorentz force is parallel to the  $x$ -axis. If the inertial force is negligible, then the equation motion of the vortex is given by

$$\eta \dot{u} + \kappa u = \mathbf{F}(z, \tau) \cdot \mathbf{e}_x, \quad (\text{A4})$$

where  $u$  is the displacement of the vortex along the  $x$ -axis,  $\eta$  and  $\kappa$  are the viscous drag coefficient, and the coefficient of the restoring force per unit length of the magnetic vortex, respectively. By solving the equation of motion, the vortex displacement is expressed as

$$u(z, \tau) = \frac{h_0 \phi_0}{\lambda_z (\kappa - i\omega\eta)} e^{-\frac{z}{\lambda_z}} e^{-i\omega\tau}. \quad (\text{A5})$$

The motion of the vortex induces an electric field  $\mathbf{E} = \mathbf{B} \times \mathbf{v}$ , where  $\mathbf{v}$  is the velocity of the vortex. From Faraday's law, given by  $\partial \mathbf{B} / \partial \tau = -\nabla \times \mathbf{E}$ , the temporal change in the magnetic field due to the motion-induced electric field is given by

$$\frac{\partial \mathbf{B}}{\partial \tau} = -\nabla \times (\mathbf{B} \times \mathbf{v}). \quad (\text{A6})$$

The vortex density changes owing to the motion caused by the Lorentz force. Accordingly, the magnetic flux density also changes, and it can be expressed as a summation of the external magnetic flux density  $\mathbf{B}_0$  and the additional magnetic flux density  $\mathbf{b}_v$ , which oscillates with frequency  $\omega$ . Substituting  $\mathbf{B}_0 + \mathbf{b}_v$  into  $\mathbf{B}$  and integrating with respect to time yields

$$\mathbf{b}_v = -\nabla \times (\mathbf{B}_0 \times u(z, \tau) \mathbf{e}_x). \quad (\text{A7})$$

As a result, the induced magnetic and electric fields are respectively given by

$$\mathbf{b}_v(z, \tau) = -B_0 \frac{\partial u(z, \tau)}{\partial z} \mathbf{e}_x, \quad (\text{A8})$$

$$\mathbf{E}(z, \tau) = i\omega \mu_0 h_0 \lambda_x e^{-\frac{z}{\lambda_z}} e^{-i\omega\tau} \mathbf{e}_y, \quad (\text{A9})$$

where  $B_0 = |\mathbf{B}_0|$ .

According to Faraday's law, a magnetic flux density that originates in the motion-induced electric field  $\mathbf{b}(x, \tau) = i\nabla \times \mathbf{E} / \omega$  is generated. Two magnetic flux densities,  $\mathbf{b}$  and  $\mathbf{b}_v$ , are connected to the current density by the London equation

$$\nabla \times \mathbf{J} = -\frac{1}{\mu_0 \lambda_L^2} (\mathbf{b}(x, \tau) - \mathbf{b}_v(z, \tau)). \quad (\text{A10})$$

By integrating both sides of Equation (A10) with respect to  $z$ , we have the current density parallel to the  $y$ -axis, which is the second expression,

$$J_y = -\frac{1}{\mu_0 \lambda_L^2} \left( \frac{i}{\omega} E + B_0 u(z, \tau) \right). \quad (\text{A11})$$

By combining Equations (A2) and (A11), the following relationship between  $\lambda_z$  and  $\lambda_L$  is obtained:

$$\lambda_z^2 = \lambda_L^2 + \frac{B_0\phi_0}{\mu_0(\kappa - i\omega\eta)}. \quad (\text{A12})$$

This is how the penetration depth in Equation (21) was derived.

## References

1. Stange, A.; Campbell, D.K.; Bishop, D.J. Science and technology of the Casimir effect. *Phys. Today* **2021**, *74*, 42–48. [[CrossRef](#)]
2. Lamoreaux, S.K. Demonstration of the Casimir force in the 0.6 to 6  $\mu\text{m}$  range. *Phys. Rev. Lett.* **1997**, *78*, 5–8. [[CrossRef](#)]
3. Milonni, P.W. *The Quantum Vacuum*; Academic Press: San Diego, CA, USA, 1994.
4. Bordag, M.; Klimchitskaya, G.L.; Mohideen, U.; Mostepanenko, V.M. *Advances in the Casimir Effect*; Oxford University Press: New York, NY, USA, 2009.
5. Casimir, H.B.G. On the attraction between two perfectly conducting plates. *Proc. Kon. Ned. Akad. Wet.* **1948**, *51*, 793–795.
6. Mohideen, U.; Roy, A. Precision Measurement of the Casimir Force from 0.1 to 0.9  $\mu\text{m}$ . *Phys. Rev. Lett.* **1998**, *81*, 4549–4552. [[CrossRef](#)]
7. Banishev, A.A.; Chang, C.C.; Klimchitskaya, G.L.; Mostepanenko, V.M.; Mohideen, U. Measurement of the gradient of the Casimir force between a nonmagnetic gold sphere and a magnetic nickel plate. *Phys. Rev. B* **2012**, *85*, 195422. [[CrossRef](#)]
8. Banishev, A.A.; Klimchitskaya, G.L.; Mostepanenko, V.M.; Mohideen, U. Casimir interaction between two magnetic metals in comparison with nonmagnetic test bodies. *Phys. Rev. B* **2013**, *88*, 155410. [[CrossRef](#)]
9. Rosa, F.S.S.; Dalvit, D.A.R.; Milonni, P.W. Casimir-Lifshitz theory and metamaterials. *Phys. Rev. Lett.* **2008**, *100*, 183602. [[CrossRef](#)]
10. Bimonte, G.; Calloni, E.; Esposito, G.; Milano, L.; Rosa, L. Towards measuring variations of Casimir energy by a superconducting cavity. *Phys. Rev. Lett.* **2005**, *94*, 180402. [[CrossRef](#)]
11. Bimonte, G.; Calloni, E.; Esposito, G.; Rosa, L. Variations of Casimir energy from a superconducting transition. *Nuc. Phys. B* **2005**, *726*, 441–463. [[CrossRef](#)]
12. Bimonte, G. Casimir effect in a superconducting cavity and the thermal controversy. *Phys. Rev. A* **2008**, *78*, 062101. [[CrossRef](#)]
13. Sushkov, A.O.; Kim, W.J.; Dalvit, D.A.R.; Lamoreaux, S.K. Observation of the thermal Casimir force. *Nat. Phys.* **2011**, *7*, 230–233. [[CrossRef](#)]
14. Klimchitskaya, G.L.; Mostepanenko, V.M. Recent measurements of the Casimir force: Comparison between experiment and theory *Mod. Phys. Lett.* **2020**, *35*, 2040007. [[CrossRef](#)]
15. Perez-Morelo, D.; Stange, A.; Lally, R.W.; Barrett, L.K.; Imboden, M.; Som, A.; Campbell, D.K.; Aksyuk, V.A.; Bishop, D.J. A system for probing Casimir energy corrections to the condensation energy. *Microsyst. Nanoeng.* **2020**, *6*, 115. [[CrossRef](#)] [[PubMed](#)]
16. Norte, R.A.; Forsch, M.; Wallucks, A.; Marinković, I.; Gröblacher S. Platform for Measurements of the Casimir Force between Two Superconductors. *Phys. Rev. Lett.* **2018**, *121*, 030405. [[CrossRef](#)]
17. Bimonte, G. Casimir effect between superconductors. *Phys. Rev. A* **2019**, *99*, 052507. [[CrossRef](#)]
18. Quach, J.Q. Gravitational Casimir Effect. *Phys. Rev. Lett.* **2015**, *114*, 081104. [[CrossRef](#)]
19. Golosovsky, M.; Tsindlekht, M.; Davidov, D. High-frequency vortex dynamics in  $\text{YBa}_2\text{Cu}_3\text{O}_7$ . *Supercond. Sci. Technol.* **1996**, *9*, 1–7. [[CrossRef](#)]
20. Brandt, E.H. Penetration of magnetic ac fields into type-II superconductors. *Phys. Rev. Lett.* **1991**, *67*, 2219–2222. [[CrossRef](#)]
21. Kogan, V. G.; Nakagawa, N. Current distributions by moving vortices in superconductors *Phys. Rev. B* **2021**, *103*, 134511. [[CrossRef](#)]
22. Kogan, V. G.; Nakagawa, N. Moving vortices in anisotropic superconductors *Phys. Rev. B* **2021**, *104*, 094523. [[CrossRef](#)]
23. Villarreal, C.; Caballero-Benitez, S.F. Casimir forces and high-Tc superconductors. *Phys. Rev. A* **2019**, *100*, 042504. [[CrossRef](#)]
24. Castillo-Lopez S.G.; Villarreal C.; Pirruccio G.; Esquivel-Sirvent, R. Role of electronic relaxation rates in the Casimir force between high-Tc superconductors. *Universe* **2021**, *7*, 69. [[CrossRef](#)]
25. Moser, E.K.; Tomasch, W.J.; McClorey, M.J.; Furdyna, J.K.; Coffey, N.W.; Pettiette-Hall, C.L.; Schwarzbeck, S.M. Microwave properties of  $\text{YBa}_2\text{Cu}_3\text{O}_{7-x}$  films at 35 GHz from magnetotransmission and magnetoreflexion measurements. *Phys. Rev. B* **1994**, *49*, 4199–4208. [[CrossRef](#)] [[PubMed](#)]
26. Coffey, M.W.; Clem, J.R. Magnetic field dependence of RF surface impedance. *IEEE Trans. Mag.* **1991**, *27*, 2136–2139. [[CrossRef](#)]
27. Coffey, M.W.; Clem, J.R. Unified theory of effects of vortex pinning and flux creep upon the rf surface impedance of type-II superconductors. *Phys. Rev. Lett.* **1991**, *67*, 386–389. [[CrossRef](#)]
28. Coffey, M.W.; Clem, J.R. Theory of microwave transmission and reflection in type-II superconductors in the mixed state. *Phys. Rev. B* **1993**, *48*, 342–350. [[CrossRef](#)]
29. Lifshitz, E.M. The theory of molecular attractive forces between solids. *Sov. Phys. JETP* **1956**, *2*, 73–83.
30. Greenaway, D.L.; Harbeke, G.; Bassani, F.; Tosatti, E. *Phys. Rev.* Anisotropy of the Optical Constants and the Band Structure of Graphite. **1969**, *178*, 1340–1348. [[CrossRef](#)]
31. Tinkham, M. Energy gap interpretation of experiments on infrared transmission through superconducting films. *Phys. Rev.* **1956**, *104*, 845. [[CrossRef](#)]

32. Kubo, R. Statistical-mechanical theory of irreversible processes. I. general theory and simple applications to magnetic and conduction problems. *J. Phys. Soc. Jpn* **1957**, *12*, 570–586. [[CrossRef](#)]
33. Wu, D.-H.; Sridhar, S. Pinning forces and lower critical fields in  $\text{YBa}_2\text{Cu}_3\text{O}_y$  crystals: temperature dependence and anisotropy. *Phys. Rev. Lett.* **1990**, *65*, 2074–2077. [[CrossRef](#)]
34. Bonn, D.A.; O'Reilly, A.H.; Greedan, J.E.; Stager, C.V.; Timusk, T.; Kamaras, K.; Tanner, D.B. Far-infrared properties of ab-plane oriented  $\text{YBa}_2\text{Cu}_3\text{O}_7$ . *Phys. Rev. B* **1988**, *37*, 1574–1579. [[CrossRef](#)] [[PubMed](#)]
35. Coffey, M.W.; Clem, J.R. Theory of rf magnetic permeability of type-II superconductors in slab geometry with an oblique applied static magnetic field. *Phys. Rev. B* **1992**, *45*, 10527–10535. [[CrossRef](#)]
36. Bezerra, V.B.; Klimchitskaya, G.L.; Romero, C. *Phys. Rev. A* **2001**, *65*, 012111. [[CrossRef](#)]
37. Gong, T.; Corrado, M.R.; Mahbub, A.R.; Shelden, C.; Munday, J.N. Recent progress in engineering the Casimir effect? Applications to nanophotonics, nanomechanics, and chemistry. *Nanophotonics* **2021**, *10*, 523–536. [[CrossRef](#)]
38. Chen, F.; Klimchitskaya, G.L.; Mostepanenko, V.M.; Mohideen, U. Control of the Casimir force by the modification of dielectric properties with light. *Phys. Rev. B* **2007**, *76*, 035338. [[CrossRef](#)]
39. Iannuzzi, D.; Lisanti, M.; Capasso, F. Effect of hydrogen-switchable mirrors on the Casimir force. *Proc. Natl. Acad. Sci. USA* **2004**, *101*, 4019–4023. [[CrossRef](#)] [[PubMed](#)]